ChemPubSoc Europe

DOI: 10.1002/chem.201600859

CHEMISTRY
A European Journal
Full Paper

Fluorescence Enhancement

Hydrogen-Bond and Supramolecular-Contact Mediated Fluorescence Enhancement of Electrochromic Azomethines

Monika Wałęsa-Chorab,[a, b] Marie-Hélène Tremblay,[a] and William G. Skene*[a]

Abstract: An electronic push–pull fluorophore consisting of an intrinsically fluorescent central fluorene capped with two diaminophenyl groups was prepared. An aminothiophene was conjugated to the two flanking diphenylamines through a fluorescent quenching azomethine bond. X-ray crystallographic analysis confirmed that the fluorophore formed multiple intermolecular supramolecular bonds. It formed two hydrogen bonds involving a terminal amine, resulting in an antiparallel supramolecular dimer. Hydrogen bonding was also confirmed by FTIR and NMR spectroscopic analyses, and further validated theoretically by DFT calculations. Intrinsic fluorescence quenching modes could be reduced by intermolecular supramolecular contacts. These contacts could be engaged at high concentrations and in thin films, resulting in fluorescence enhancement. The fluorescence of the fluorophore could also be restored to an intensity similar to its azomethine-free counterpart with the addition of water in $>50\%$ v/v in tetrahydrofuran (THF), dimethyl sulfoxide (DMSO), and acetonitrile. The fluorophore also exhibited reversible oxidation and its color could be switched between yellow and blue when oxidized. Reversible electrochemically mediated fluorescence turn-off on turn-on was also possible.

Introduction

Conjugated azomethines have attracted much attention in part because of their straightforward preparation. This has been further spurred by their properties, which are ideally suited for use as functional materials in plastic electronics. For example, conjugated derivatives have been successfully used as active layers in organic photovoltaics[1] and electrochromic devices.[1c,2] Although property tailoring is possible through the judicious selection of aromatics used for their preparation, a key azomethine property that remains elusive is high fluorescence quantum yields (Φ_{fl}). Their quenched fluorescence has proven to be a major impediment for azomethine use in high-performance emitting applications.

The principal intrinsic deactivation pathways responsible for conjugated azomethine fluorescence quenching are photoinduced electron transfer and photoisomerization between the *E*- and *Z*-isomers.[3] Although no net photoproducts are formed because the *Z*-isomer thermally isomerizes to the thermodynamically *E*-isomer,[4] $E \rightarrow Z$ isomerization is nonetheless an efficient quenching manifold. Current strategies to suppress these energy-dissipating excited-state modes involve structural modification. These include metal coordination[5] and incorporating hydroxyl groups that sustain excited-state intramolecular proton transfer.[6] Although these are efficient means for fluorescence enhancement, they significantly alter the azomethines properties. It would therefore be beneficial to use other strategies for fluorescence enhancement, especially those that do not alter the intrinsic spectroscopic, electronic, or electrochemical properties.

Typically, fluorophore fluorescence decreases with increasing concentration. This is in part because of screening effects and intermolecular quenching. In contrast, in aggregation-induced emission (AIE), the fluorescence is enhanced with increasing concentration.[7] This is a result of intermolecular interactions that suppress intrinsic molecular motions that deactivate the excited state.[8] AIE enhancement has recently been demonstrated as a viable means of suppressing otherwise fluorescence deactivation modes, especially in thin films and crystals.[9] This has been beneficial for enhancing the performance and color emitted from organic light-emitting devices.[9b,10] AIE enhancement has also been used for field-effect transistors,[11] sensors,[7b] and memory devices.[12] AIE enhancement is therefore a viable process for restoring the fluorescence of otherwise nonfluorescent azomethines.

AIE has proven useful for suppressing the inherent emission deactivation modes of azomethines and for increasing their fluorescence. The emission enhancement modes have principally been from aromatic stacking[13] or weak binding of an analyte.[14] Although it was recently demonstrated that supramolecular contacts that drive crystallization in the solid state can be used for AIE enhancement,[15] only a limited number of examples have used such contacts for enhancing the fluores-

[a] Dr. M. Wałęsa-Chorab, M.-H. Tremblay, Prof. Dr. W. G. Skene
Laboratoire de caractérisation photophysique des matériaux conjugués
Département de chimie, Université de Montréal
CP 6128, Centre-ville Montreal, QC (Canada)
E-mail: w.skene@umontreal.ca

[b] Dr. M. Wałęsa-Chorab
Current address:
Faculty of Chemistry, Adam Mickiewicz University
Umultowska 89b, 61-614 Poznań (country/>Poland)

Supporting information for this article and ORCID are available on the WWW under http://dx.doi.org/10.1002/chem.201600859.

cence of azomethines. These have relied on the imine nitrogen to promote intermolecular =N···HS–[16] and =N···HC–[17] bonds in addition to intramolecular =N···HO–[17] supramolecular contacts.

Terminal NH_2 groups would be ideal scaffolds for mediating hydrogen bonding and enhancing azomethine fluorescence. More importantly, such supramolecular contacts would be beneficial for promoting lateral fluorophore interactions for ultimately generating smooth and homogenous fluorescent thin films. While supramolecular assembly mediated by hydrogen bonds is well-known,[18] it remains relatively unexplored for promoting azomethine fluorescence. We were therefore motivated to prepare conjugated azomethines that could promote lateral intermolecular hydrogen bonds and other supramolecular contacts for fluorescence enhancement. The fluorophore shown in Figure 1 was targeted to demonstrate such an AIE

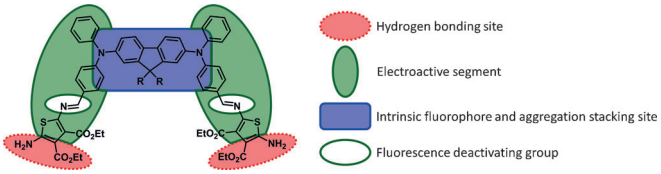

Figure 1. Electrochromic azomethine prepared and examined for AIE enhancement driven by intermolecular supramolecular contacts.

enhancement. It is an interesting fluorophore for investigating AIE, in part because azomethines derived from its end-capped 2,5-diaminothiophene are known to have quenched fluorescence.[19] It therefore should minimally fluoresce. Its fluorene core serves as the intrinsic fluorophore, the quenched fluorescence of which should be enhanced upon reducing the azomethine deactivation modes. This should be possible by engaging concentration-mediated supramolecular contacts, involving lateral intermolecular hydrogen bonding through the terminal amines. The two amine–azomethine–phenylamine arms are further expected to form a cleft for additional intermolecular contacts to reinforce the AIE. Moreover, the terminal amines are expected to contribute to the donor–acceptor–donor electronic arrangement of the amine–azomethine–phenylamine structure, resulting in interesting spectroscopic and electrochemical properties. The conjugated arm is further expected to be electroactive, with reversible oxidation and color switching between the neutral and oxidized states. The collective fluorescent and electrochemical properties would also make the fluorophore an ideal candidate for electrochemically induced fluorescence switching. The crystallographic structure, fluorescence, electrochemical, spectroelectrochemical, and fluoroelectrochemical properties of the azomethine fluorophores **1** and **2** (Scheme 1) are herein presented to demonstrate concentration-activated supramolecular contacts for mediating fluorescence enhancement.

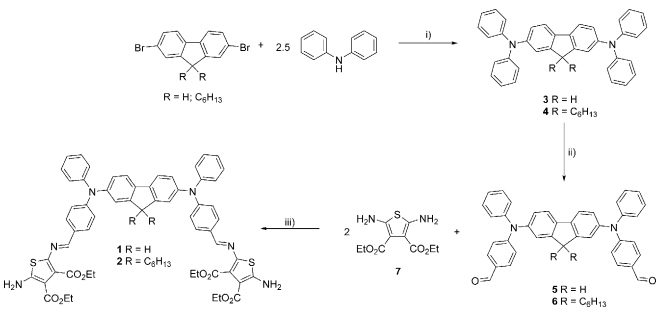

Scheme 1. Preparation of the fluorenylazomethine. Reagents and conditions: i) $Pd(OAc)_2$, tBu_3P, $CsCO_3$, toluene, 120 °C, 24 h; ii) $POCl_3$, DMF, dichloroethane, reflux, 15 h; iii) TFA, EtOH, 80 °C, 15 h.

Results and Discussion

The fluorene–triphenylamine–dialdehyde precursors **5** and **6** were prepared in a multistep synthesis as per Scheme 1. The corresponding 2,7-dibromofluorene was reacted with diphenylamine in a Pd-catalyzed N-arylation reaction, followed by standard Vilsmeier–Haack formylation. Condensation of **5** and **6** with 2,5-diaminothiophene **7** in ethanol with catalytic trifluoroacetic acid resulted in the targeted azomethines **1** and **2**, respectively.

Although the structures of both **1** and **2** were confirmed by conventional characterization methods, unequivocal evidence was sought by X-ray crystallography. The added benefit of crystallography is that both intra- and intermolecular supramolecular bonding can be confirmed. For this reason, crystals of the electrochromes were pursued. Crystals suitable for X-ray diffraction were obtained by the slow diffusion of diisopropyl ether into a dichloromethane solution of **1**. Crystals of **2** for X-ray diffraction could not be obtained because of the high degree of disorder from the alkyls groups of the fluorene core. The resolved X-ray structure shown in Figure 2 (top panel)

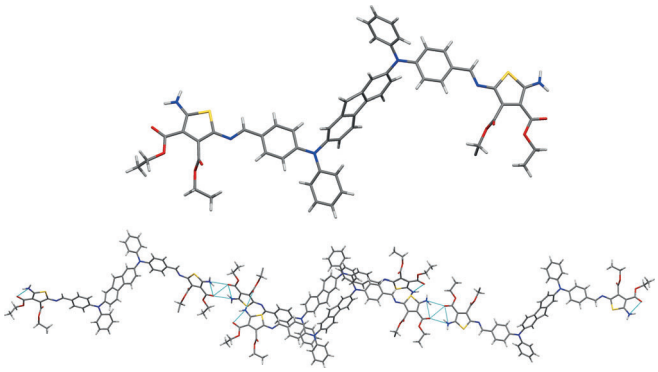

Figure 2. Resolved X-ray structure of **1** (top). Crystal packing of **1** illustrating the inter- and intramolecular hydrogen bonds drawn as blue lines (bottom). The solvent molecules were removed from the figures for clarity.

clearly confirms the structure of **1**. Four molecules of **1** were found to occupy the unit cell in the $P2_1/c$ space group. On the molecular level, the crystal structure also confirms the *E*-configuration of both imines. Other salient features of the resolved structure are the antiparallel arrangement of the triphenylamines and the planes described by the central fluorene and its adjacent phenylamines connected to the azomethines. These

were found to be twisted by 65.0° for one arm and 75.6° for the other arm. In this configuration, the terminal amines are oriented in up and down directions from the central fluorene along the *c*-axis, leading to a zigzag arrangement of the arms. Meanwhile, the two planes described by the terminal thiophenes were found to be twisted by 21(4)° from each other. The collective arrangements are ideal for extended hydrogen bonding of the terminal amines of the different molecules in the crystal structure, leading to linear and parallel supramolecular ribbons (see below). The triarylamines were also found to be planar, rather than the expected tetrahedral configuration. The planar arrangement is supported by the sum of the three amine angles being equal to 359.9(10)°. This is most likely due to steric and electronic effects. Of importance is the coplanarity of the aminothiophene–azomethine–phenylamine moieties in the two arms of **1**. In this configuration, the arms are expected to be highly conjugated and its donor–acceptor–donor arrangement should be sensitive to solvent effects. This would result in pronounced solvatochromic effects.

Both intra- and intermolecular supramolecular contacts could be confirmed by X-ray crystallography. In fact, multiple hydrogen bonds and other supramolecular contacts were found for **1**. Of importance are the hydrogen bonds. Intramolecular hydrogen-bonding was found between the ester carbonyl and the amine of the terminal thiophenes. This is illustrated by the blue lines in the termini of **1** in Figure 2 (bottom). The terminal amines were also found to undergo intermolecular hydrogen-bonding. Similar to the intramolecular bonding, intermolecular hydrogen-bonding occurred between the thiophene amine and the ester carbonyl. Two such bonds take place between one terminus of two different molecules of **1**, as seen in Figure 2. The intramolecular donor–acceptor bond distances were found to be similar (2.80(3) Å). The resulting hydrogen-bonded dimer places the thiophenes in a coplanar and antiparallel arrangement, having $-x$, $-y$, $1-z$ symmetry with respect to each other. The intermolecular supramolecular dimer donor–acceptor distances were found to be 2.96(2) Å. This results in a supramolecular zigzag type ribbon illustrated in the bottom panel of Figure 2. The other ester of the terminal thiophene also undergoes intermolecular hydrogen-bonding. In this case, the intermolecular contact is perpendicular to the plane described by the thiophene–imine–phenyl and involves the NH_2 of a third molecule of **1** through a $1-x$, $-1/2+y$, $3/2-z$ symmetry. The NH···OC bond distance was calculated to be 2.25(5) Å, whereas the N···O distance was 3.09(2) Å. Multiple supramolecular contacts also occurred between the first and third molecules of **1**. For example, edge-on contact between the two fluorenes, S···thiophene, S···C=O, C=O···HC=N, C=O···HC_{phenyl}, and phenyl···phenyl contacts were found. In this arrangement, the two molecules are nearly perpendicular, with the planes described by the two fluorenes found to be twisted by 76.3°. The collective X-ray data confirm that **1** has multiple intermolecular contacts. The resulting extended supramolecular structure is expected to suppress otherwise fluorescence-deactivation modes, resulting in concentration-induced fluorescence turn-on.

Although extensive supramolecular contacts were confirmed in the solid state by X-ray crystallography, such intermolecular hydrogen-bonding may not necessarily occur in solution. Concentration-dependent NMR studies between 0.8 and 50 mM were therefore undertaken to probe whether intermolecular hydrogen-bonding occurred in solution. The distinct chemical shift of the NH_2 protons did not overlap with other protons. This made it an ideal signal for probing concentration-induced intermolecular hydrogen-bonding. The NH_2 signal, which was assigned based on 2D HMBC experiments (Supporting Information, Figure S13), was expected to shift downfield with increasing concentration with hydrogen bonding. As seen in Figure 3, the chemical shift of the amine protons is shifted

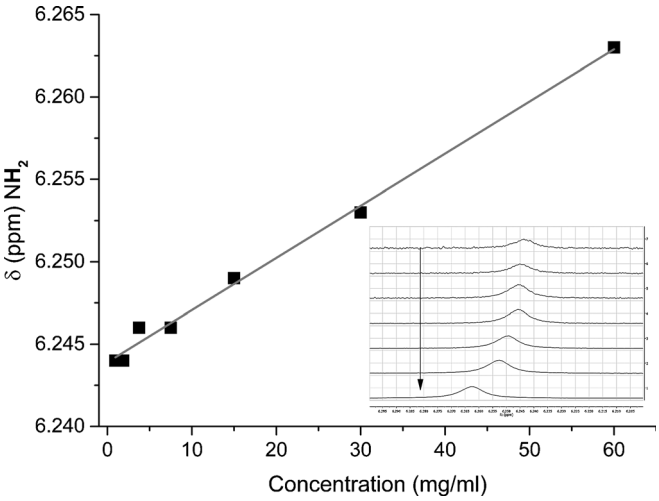

Figure 3. Chemical shifts of the NH_2 protons **2** as a function of concentration in $CDCl_3$ (0.8 to 50 mM) Inset: NMR spectra of the NH_2 protons of **2** with increasing concentration in $CDCl_3$ from top to bottom.

with increasing concentration of **2** in anhydrous $CDCl_3$. In fact, a linear correlation ($r^2 = 0.993$) of chemical shift to higher frequencies contingent on concentration was observed. The NMR data provide sound evidence for the concentration-induced hydrogen-bonding of the terminal amines.

Infrared spectroscopy was also used to confirm intermolecular hydrogen-bonding of the fluorophores. Similar to the NMR studies, significant differences in the IR spectra were expected between the fluorophore with and without hydrogen bonding. DFT calculations were first performed. These were used to identify both the stretching frequencies involved in hydrogen bonding and to assign the experimentally measured frequencies. The X-ray crystal structure of **1** was used as the starting geometry for optimizing the DFT calculated geometry. Compound **1** was chosen for the calculations rather than **2** because of its reduced number of atoms and decreased degrees of freedom, which allowed the computational cost to be reduced. The resulting fully optimized gas-phase DFT ground-state geometry was in good agreement with the X-ray structure (Supporting Information, Figure S15).

Hydrogen bonding was calculated to occur between the electron-deficient hydrogen and a region of high electron-den-

sity. Multiple hydrogen bonds were found with **1**. The calculated interactions were intramolecular between the ester carbonyl and the terminal amine, along with intermolecular bonding between the same groups between two different molecules. These were consistent with the X-ray crystal structure. Given the intermolecular hydrogen bonds were expected to enhance the fluorescence, these were calculated in more detail.

Hydrogen bonding was expected to increase the N–H and the C=O bond lengths. The calculated intermolecular hydrogen-bond distance was 3.06 Å, consistent with the value measured by X-ray crystallography. The N–H bonds were calculated to extend by 23%, whereas the carbonyl was calculated to extend by 32%. These significant bond stretches should be noticeable in the IR spectrum. The infrared spectra of **1** both with and without hydrogen bonds were therefore calculated, with particular attention to the N–H vibrations. The asymmetric and symmetric stretching bands were found to shift with intermolecular hydrogen-bonding. The asymmetric N–H stretching at 3678 cm^{-1} decreased by 55 cm^{-1} with hydrogen bonding. The symmetric N–H stretching at 3510 cm^{-1} was also calculated to shift to lower wavenumbers by 10 cm^{-1}, albeit less than the asymmetric stretching upon hydrogen bonding (Figure 4A). The spectral shifts were also accompanied with an increase in the signal intensity. The stretching signals increased twofold, with the greatest increase found for the symmetric stretching (Supporting Information, Table S2).

The experimentally measured FTIR spectra of **2** are shown in Figure 4B. The spectra were recorded both as a highly dilute solution and as a power. These two extremes were chosen to ensure both the absence of hydrogen bonds and the hydrogen bonded forms of **2** were recorded. CCl_4 was selected as solvent for solution measurements because of its spectroscopic invisibility in the region of interest. Whereas the absolute frequencies between the measured and calculated spectra were different, their trends with hydrogen bonding were consistent. The symmetric stretching peak at 3335 cm^{-1} was reduced by 26 cm^{-1} upon hydrogen bonding. Whereas the peak at 3430 cm^{-1} was found not to significantly shift, its intensity increased 2.7-fold, compared with the symmetric stretching peak with hydrogen bonding. This is consistent with the theoretical calculations. The collective FTIR and NMR concentration-dependence studies confirm that concentration-mediated intermolecular hydrogen-bonding between fluorophores occurs.

The solvatochromism of both **1** and **2** and their corresponding dialdehydes were investigated. This was done to gain insight into their fluorescence properties and to better understand their concentration-induced fluorescence properties. Both fluorophores **1** and **2** and their respective dialdehyde precursors were expected to exhibit solvent-dependent fluorescence changes. The triarylamine serves both as a basic site and electron donor. Solvent can therefore interact with the arylamine through hydrogen bonding and other electrostatic interactions. These perturb significantly the excited-state molecular dipole, resulting in strong solvent-dependent spectral changes. Similarly, the electron donor–acceptor–donor arrangement of the aminothiophene–azomethine–phenylamine configuration of **1** and **2** was further expected to be sensitive to solvent. Enhanced solvatochromic effects of **1** and **2** were therefore expected compared with their corresponding analogues **5** and **6**.

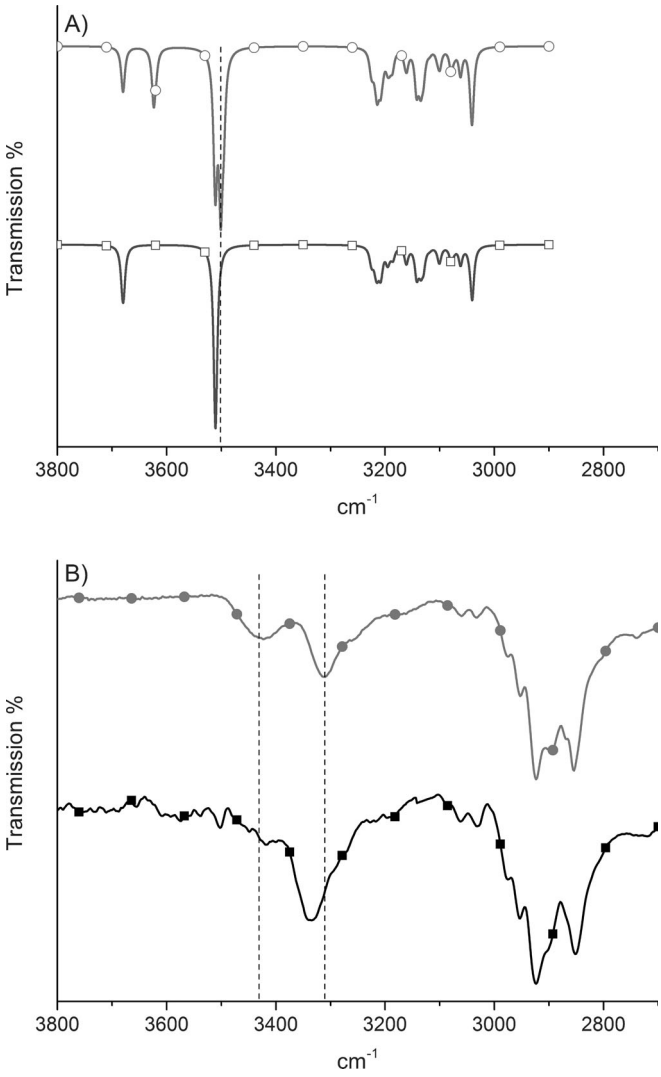

Figure 4. A) Calculated DFT IR spectra of **1** with (○) and without (□) hydrogen bonding. B) FTIR spectra of 96 μM of **2** in CCl_4 (■) and as a powder (●).

As seen in Figure 5A, the fluorescence of **2** was significantly affected by the nine solvents examined. This was also the case for **1**, **5**, and **6**. Notably, the absorption of **1**, **2**, **5**, and **6** varied by up to 5 nm in the different solvents (Supporting Information, Figures S18, S30, S41, and S53). The fluorescence change with solvent therefore reflects excited-state solvent–fluorophore interactions. For **1**, **2**, **5**, and **6**, the fluorescence was redshifted with solvent polarity upwards of 200 nm (Table 1). The fluorescence redshift with solvent polarity is consistent with a greater stabilization of the excited state relative to the ground state. The pronounced positive solvatochromism observed arises from the donor–acceptor effect of the fluorophores involving the triarylamine conjugated with the electron-accepting moiety; the carbonyl for **5** and **6**, and the azomethine for **1** and **2**. The solvatofluorochromic effects of **2** and **6** are qualitatively seen in the converging slopes in Figure 5B. The Stokes shift of the fluorophores contingent on the solvent

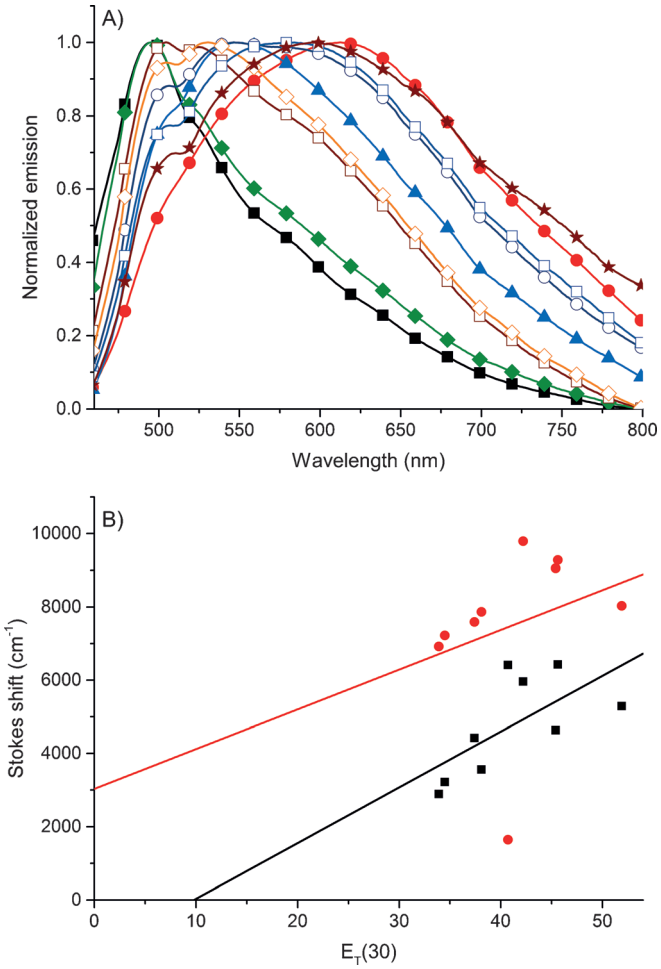

Figure 5. A) Normalized emission spectra of **2** in toluene (■), diethyl ether (◆), ethyl acetate (□), THF (◇), ethanol (○), DMSO (▲), acetone (□), dichloromethane (●) and acetonitrile (⋆) at 1.0 μM. B) Stokes shift of **2** (■) and **6** (●) as a function of solvent E_T(30) parameter.

Table 1. Selected photophysical data.

Solvent	η[a]	1		2		5		6	
		λ_{fl} [nm][b]	Φ_{fl} [%][c]	λ_{fl} [nm][b]	Φ_{fl} [%][c]	λ_{fl} [nm][b]	Φ_{fl} [%][c]	λ_{fl} [nm][b]	Φ_{fl} [%][c]
CH_2Cl_2	1.424	585	0.22	613	0.25	403	1.44	403	1.65
toluene	1.497	495	0.09	495	0.11	518	36.7	463/523	39.0
Et_2O	1.352	495	0.06	495	0.08	515	26.4	520	31.0
EtOAc	1.371	515	0.11	505	0.11	545	5.69	536	9.34
EtOH	1.361	545	0.12	560	0.13	426/547	0.12	426/549	0.19
acetone	1.359	550	0.11	580	0.12	608	0.19	595	0.35
THF	1.407	525	0.11	531	0.19	545	9.63	536	16.0
acetonitrile	1.344	570	0.08	600	0.09	426/600	0.05	426/575	0.08
DMSO	1.479	545	0.21	548	0.22	426/574	0.22	426/570	0.44

[a] Refractive index taken from the literature.[22] [b] Emission maximum wavelength. [c] Reference against naphthalene (Φ_{fl} = 23% in cyclohexane).[23]

E_T(30) parameter is somewhat linear. The less than linear trend suggests specific solute–solvent interactions in addition to nonspecific interactions. This notwithstanding, the fluorescence redshift of **1** and **2** was also complemented with a broadening of the emission. This is consistent with the excited state adopting many orientations, each being perturbed by the solvent.

The fluorescence quantum yield (Φ_{fl}) of **1**, **2**, **5**, and **6** was also evaluated in the different solvents. This was to benchmark the values for concentration studies and to confirm the fluorescence quenching of the azomethine. As expected, the Φ_{fl} of **1** and **2** were consistently low (< 1%), irrespective of solvent (Table 1). The fluorescence is quenched by the azomethine bonds. In contrast, the Φ_{fl} of **5** and **6** varied markedly with solvent; they fluoresced appreciably in toluene, diethyl ether, and tetrahydrofuran (THF).

The fluorescence of the fluorophores contingent on concentration in THF was also investigated to determine whether the intermolecular interactions measured experimentally by X-ray diffraction, IR, and NMR along with the theoretically calculated hydrogen-bonding, enhanced the fluorescence as surmised. As seen in Figure 6, there was a marked effect of concentration on the spectroscopic properties. For **2** in THF, a red color was observed when the concentration was increased seven orders of magnitude, owing to an increased absorption at 540 nm. The fluorescence was redshifted with increasing concentration. The observed bathochromic shifts in both the absorption and fluorescence were assumed to be a result of increased fluorophore–fluorophore interactions. Correcting for changes in absorption, the fluorescence emission also increased with con-

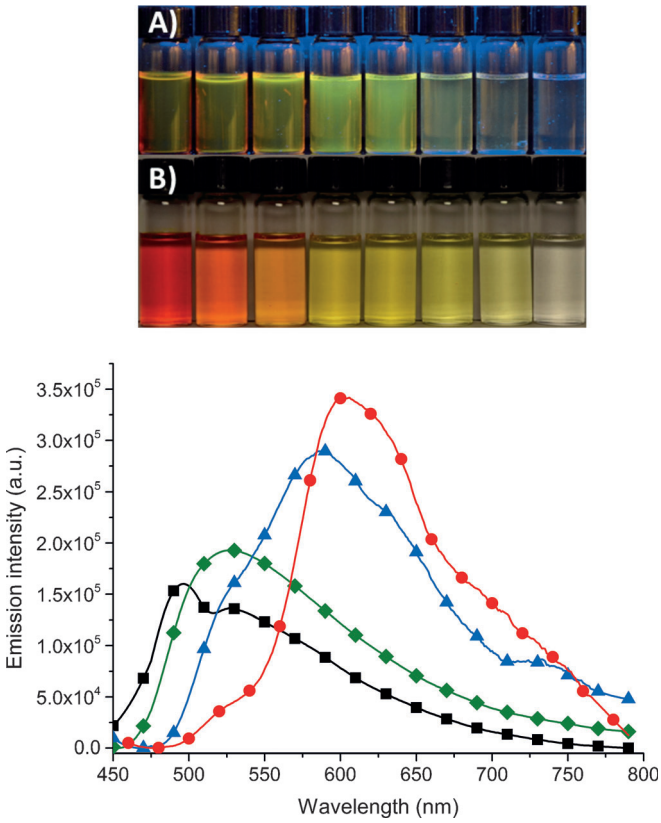

Figure 6. Top: photographs showing the fluorescence of **2** in sample vials of THF with increasing concentration (from right to left) when irradiated with a UV lamp (A) and under ambient light (B). Bottom: fluorescence spectra of **2** in deoxygenated and anhydrous THF measured at $3.3 \cdot 10^{-4}$ (■), 33.3 (◆), 170 (▲), and 1000 (●) μmol L^{-1}.

centration, as per Figure 6. In fact, the fluorescence increased twofold with increasing concentration. This suggests that otherwise intrinsic fluorescence deactivation modes are diminished with intermolecular supramolecular contacts between the azomethines. The observed bathochromic shift with increasing concentration along with the increased fluorescence are further consistent with the formation of *J*-type aggregates.[20] In contrast, *H*-type aggregates would result in hypsochromic shifts and decreased emission with increasing concentration.[21]

The concentration-dependent fluorescence of **2** was also examined in thin films. This was to evaluate the fluorescence behavior with varying degrees of intermolecular interactions in the solid state. For this, **2** was cast on glass slides from a stock solution in dichloromethane. The azomethine was also mixed in varying weight% ratios with poly(methyl methacrylate) (PMMA) in dichloromethane. This polymer was chosen because it is miscible with **2** and it does not phase separate. It also forms a uniform and homogenous film on glass. This property is key for accurate fluorescent measurement. The dependence of emission wavelength on the concentration of **2** in thin films (Figure 7) was consistent with what was observed in solution.

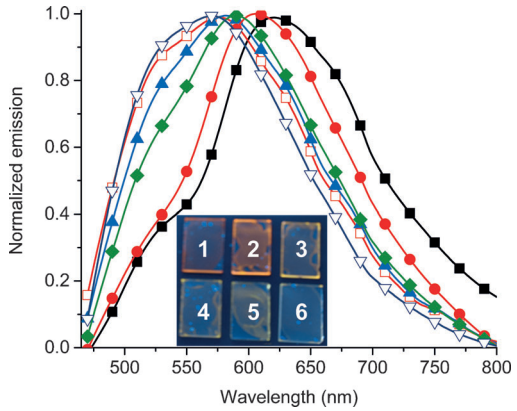

Figure 7. Normalized emission spectra of thin films of **2** in 1:0 (■), 1:10 (●), 1:30 (◆), 1:50 (▲), 1:80 (□), and 1:100 (▽) weight ratios in a PMMA matrix. Inset: pictures showing the emission of **2** in thin films cast on glass substrates when irradiated with a UV lamp in 1:0 (**1**), 1:10 (**2**), 1:30 (**3**), 1:50 (**4**), 1:80 (**5**), 1:100 (**6**) weight ratios in a PMMA matrix.

For example, the most blueshifted fluorescence was observed when **2** was the most dilute in the PMMA matrix (1:100 wt% PMMA). Under these conditions, the lowest number of intramolecular contacts occur. The measured fluorescence of **2** in the 1:100 wt% PMMA film was redshifted by 75 nm compared with what was measured at 3.3×10^{-4} M. This implies that **2** forms intermolecular contacts even when dispersed in the PMMA matrix. With increasing wt% of **2** in the PMMA matrix, its fluorescence was redshifted, owing to the increased number of intermolecular contacts. The same emission was observed for both the as-cast thin film from a stock solution without the PMMA matrix and in a 1000 μM solution. The effect of concentration of **2** in thin films on the color emitted and emission intensity can qualitatively be seen in the photographs in Figure 7. Quantitatively, the fluorescence was redshifted upwards of 100 nm and its fluorescence emission increased 2.6-fold. Owing to differences in thin-film thickness and limitations of relative actinometry, only relative emission yields could be obtained. Notably, the intrinsic fluorescence is typically quenched when fluorophores are cast as films and when not embedded in a matrix. Bearing this in mind, the enhanced fluorescence observed with **2** in thin film provides further evidence for intermolecular interactions that reduces the otherwise efficient azomethine fluorescence quenching modes.

To examine whether the azomethines underwent the proposed enhanced AIE when aggregated in solution, the fluorescence of **1** and **2** were measured in THF, acetonitrile, and dimethyl sulfoxide (DMSO) with varying amounts of water. These organic solvents were chosen because of their miscibility with water. Given the poor hydrophilic character of the azomethines, especially **2** owing the fluorene alkyl groups, the addition of water should aggregate **1** and **2**. Redshifted fluorescence concomitant with a fluorescence enhancement should both be observed with aggregate formation upon the addition of water. As seen in Figure 8A, the fluorescence behavior of **2**

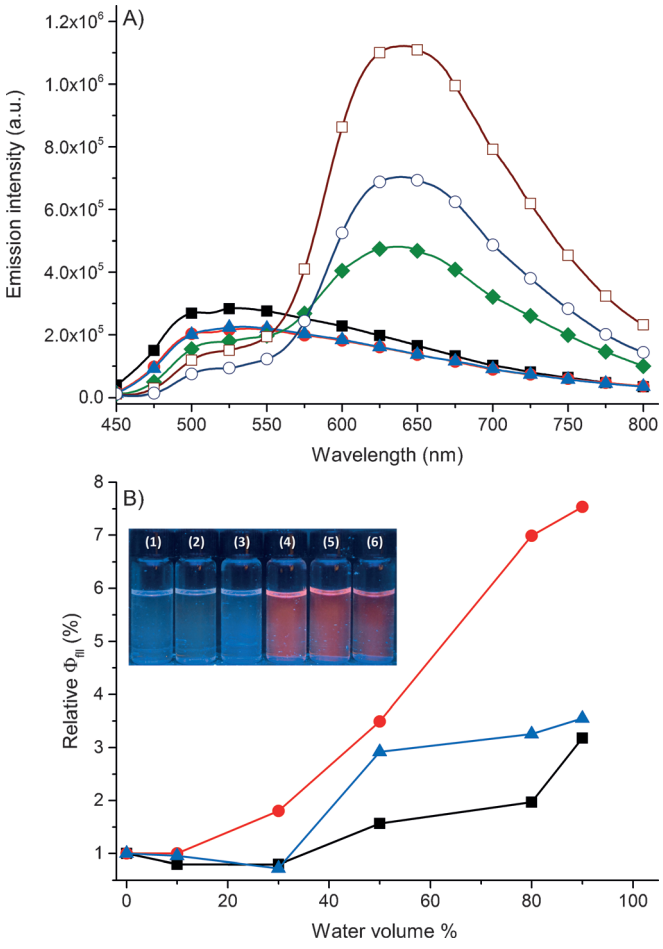

Figure 8. A) Fluorescence spectra of **2** in THF with different volume% of water: 0% (■), 10% (▲), 30% (●), 50% (◆), 80% (○), and 90% (□). B) Relative quantum yield of **2** in THF (■), acetonitrile (●), and DMSO (▲) with varying volume% of water. Inset: photographs showing the fluorescence of **2** in vials of DMSO when irradiated with a UV lamp with 0 (A), 10 (B), 30 (C), 50 (D), 80 (E), and 90 (F) volume% of water.

was markedly dependent on water being added to the environment. The fluorescence intensity decreases somewhat with increasing amounts of water, in part due to variations in the sample volume. This aside, the fluorescence emission redshifted by 130 nm once the water content was greater than 50%. Subsequent addition of water increased the fluorescence intensity. In fact, the fluorescence increased eightfold with water. The fluorescence of **1** and **2** measured, once the water volume% threshold was met, was similar to what was measured at high concentrations in homogenous solutions. For the absorption, no appreciable shifts were observed for the principle absorption at 432 nm upon the addition of water. Only the absorption at 458 nm was water sensitive: it decreased by up to 16% relative to the peak at 432 nm for both **1** and **2** upon the addition of water (Supporting Information, Figures S21, S24, S27, S32, S33, and S36). Given the absorptions of **5** and **6** were centered at 380 nm and varied only by ± 5 nm with solvent (Supporting Information, Figures S41 and S53), the decrease in the absorption at 458 nm of **1** and **2** with water is unlikely to result from the azomethine bonds being hydrolyzed. The same behavior of fluorescence redshift and fluorescence enhancement with water was also observed for both DMSO and acetonitrile. The stark shift in both fluorescence wavelength and intensity of **2** in DMSO with water are evident in the photographs in Figure 8B. The measured Φ_{fl} of **1** and **2** in aggregated acetonitrile and DMSO with water was consistent for those measured for **5** and **6** in the corresponding neat solvents (Table 1). Under similar aggregation conditions, the fluorescence enhancement of **5** and **6** in THF increased only 1.5-fold. In contrast, their fluorescence in DMSO and acetonitrile water mixtures was enhanced between 2.3-fold and 5-fold, respectively, more than their azomethine counterparts under similar aggregation conditions. The emission of **5** and **6** were blueshifted by about 110 nm relative to **1** and **2** under similar conditions with added water. The collective spectroscopic data provide evidence for the formation of intermolecular fluorophore interactions that are engaged upon water addition. Although the intrinsic fluorescence of the fluorene core cannot be completely restored with the azomethine supramolecular contacts, the amount of fluorescence quenching can nonetheless be decreased, resulting in fluorescence enhancement. Restoring the inherent fluorescence of the fluorophore would require complementary means to fully suppress the efficient fluorescence quenching modes, which is believed to involve photoinduced electron transfer. Suppressing this deactivation mode would be possible by adjusting the energy levels of the fluorophore and the azomethine to make the process endergonic, as per the Rehm–Weller relationship.[24]

Time-dependent (TD) DFT theoretical calculations were performed to validate the observed intermolecular contact mediated spectral changes. The effect of hydrogen bonding on the excited-state dynamics and its impact on the spectroscopic properties were previously described by theoretical means.[25] It was found that spectral redshifting resulted from strengthening of the hydrogen bonds, whereas weakening of the bond caused blueshifts. The electronic transition energies and the oscillator strengths of the first five excited states of the hydrogen-bonded dimer of **1** were calculated. The corresponding values for **1** without hydrogen bonding (monomer) were also calculated as a benchmark. For all the calculated excited states, the energy levels of the hydrogen bonded **1** were lower than its corresponding monomer (Table 2). Whereas the greatest stabilization occurred with the 3rd and 4th excited states, the strongest oscillator strength was calculated for the 3rd excited state. The calculations confirm that hydrogen bonding with **1** has a strengthening effect, resulting in spectral redshifts. This is consistent with the spectroscopic data and further supports the formation of *J*-type aggregates. Moreover, the multiple transitions calculated to participate in the spectroscopic properties imply the spectra of the hydrogen-bonded fluorophore should be broad and not well-defined. This is consistent with the spectra experimentally measured at high concentration.

Table 2. Calculated electronic transition energies and oscillator strengths of **1**.

Excited state	Monomer		Dimer	
	E [eV]	Oscillator strength	*E* [eV]	Oscillator strength
1	1.65	0.075	1.65	0.089
2	2.29	0.352	2.10	0.000
3	2.68	1.711	2.28	0.529
4	2.77	0.018	2.30	0.005
5	2.80	0.233	2.34	0.000

An interesting feature of **1** and **2** is their triphenylamine moiety. This is known to undergo reversible oxidation in addition to color changes between the neutral and oxidized states that can readily be tracked by the user. The extended conjugation of **1** and **2** also makes them interesting electrochromic candidates because it should enhance the color difference between their neutral and oxidized states. The anodic electrochemical properties of **1** and **2** were therefore investigated by cyclic voltammetry in various solvents. The azomethines were found to exhibit either one or two oxidation waves contingent on solvent. The oxidation was reversible in acetonitrile, dichloromethane, and THF (Figure 9A). In dichloromethane, both fluorophores exhibited two reversible one-electron oxidations.

The absorption changes and corresponding colors of **1**, **2**, **5**, and **6** with electrochemical oxidation were also examined by spectroelectrochemistry. The measurements were performed in dichloromethane because of the reversible anodic processes observed in cyclic voltammetry. Both **1** and **2** exhibited a distinct color change when oxidized. Their color switched from yellow to blue when oxidized. In the case of **2**, its absorption at 443 nm decreased with the concomitant appearance of two new absorptions upon oxidation. A well-defined peak at 595 nm and broad absorption band in the near infrared region (ca. 1375 nm) were also observed (Figure 9B). Similar spectral shifts were also observed for **1**, with absorptions at 584 and 1290 nm when it was oxidized (Figure S68). Notably, a well-defined isosbestic point was observed at 483 nm with electrochemical switching between the neutral and oxidized states.

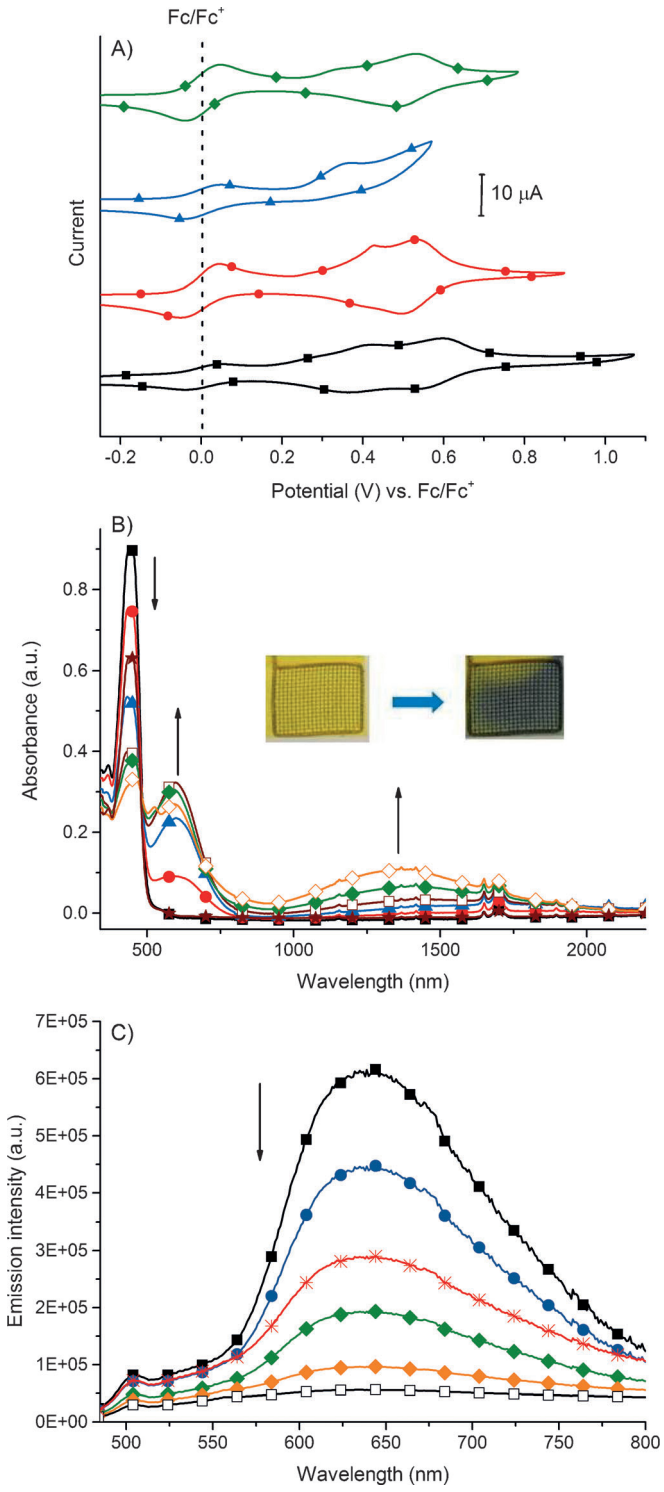

Figure 9. A) Cyclic voltammograms of **2** measured in anhydrous and deoxygenated acetone (◆), THF (▲), acetonitrile (●), and dichloromethane (■) at 100 mV s^{-1} with 0.1 M $TBAPF_6$ and ferrocene as an internal reference. B) Spectroelectrochemistry of **2** in anhydrous and deoxygenated dichloromethane with $TBAPF_6$ as an electrolyte with applied potentials of 0 (■) 700 (●), 800 (▲), 900 (□) 1000 (◆) 1100 (◇), and −500 (⋆) mV vs. Ag/Ag^+ held for 30 s per potential. Inset: photographs showing the mesh electrode of the neutral (left) and oxidized (right) states of **2**. C) Change in fluorescence of **2** in a THF/water mixture (1:9 v/v) with 0.1 M KCl as electrolyte when excited at 430 nm with applied potentials of 0 (■), 900 (●), 1100 (▲), 1200 (◆), and 1300 mV (□) for 60 s followed by −1000 mV (⋆).

This confirms the presence of only two states (neutral and oxidized) and their interdependence. Both **5** and **6** also exhibited color switching. In contrast to **1** and **2**, **5,** and **6** could be doubly oxidized (Supporting Information, Figure S67). This gives rise to two electrochemically induced color changes, one for each of the two one-electron oxidations. The two colors perceived by the user when oxidizing **5** and **6** were orange and blue (Supporting Information, Figure S69 and S70). These colors corresponded to new absorptions appearing at 690 and 1300 nm for **6**. The absorptions observed for **5** were blueshifted by 10 nm relative to **6**, with the corresponding CIE color space summarized in Table 3. The parameters in this convention quantitatively describe the colors perceived by the common user, where the L^*, a^*, and b^* parameters refer to the darkness, red/green, and yellow/blue color components, respectively.[26] Positive a^* and b^* values denote the dominance of red and yellow in the perceived color, whereas, green and blue are dominant for negative values of a^* and b^*, respectively. The illuminates refer to the lighting conditions, with A, B, C corresponding to tungsten, direct, and shady daylight, respectively. As per Table 2, the L^* value of the oxidized form of both **1** and **2** was lower than the neutral state. The perceived color of the oxidized form is therefore darker than that of the neutral state. The a^* value varied little between the neutral and oxidized forms. This confirms the conclusion that neither red nor green contribute to the perceived color. In contrast, the positive b^* value for the neutral state of **1** and **2** was significantly reduced with oxidation. The predominant yellow color perceived for the neutral form is therefore replaced with blue when **1** and **2** are oxidized, as per the inset of Figure 9B.

Given the observed fluorescence enhancement, combined with the reversible oxidation of **1** and **2**, their fluoroelectrochemistry was also investigated. This involved monitoring the fluorescence change with increasing applied potential when exciting the sample at its corresponding absorption maximum. For **1** and **2**, the excitation wavelength selected was 430 nm. Although aggregation-induced fluorescence enhancement was observed in DMSO, acetonitrile, and THF, the fluoroelectrochemistry measurements were performed in a 1:9 (v/v) mixture of THF/water. This solvent mixture was chosen because it gave the best electrochemical conductivity for the electrochemical measurements. With increasing potentials from 0 to 1.2 V, the emission at 640 nm decreased (Figure 9C). This is a result of the absorption of the neutral state being replaced with a red-shifted absorption of the oxidized state upon oxidation. Therefore, fewer neutral species are excited, resulting in the observed fluorescence decrease. Reducing the oxidized state restored the absorbance of the neutral state, which, in turn, restored the original fluorescence of the neutral state at 640 nm. This was observed by applying a negative potential to the oxidized state. The fluorescence can therefore be turned-off and turned-on electrochemically once the supramolecular contacts are activated. The same behavior was also observed for **5** and **6**, with the emission at 525 nm being modulated with applied potential.

Table 3. CIE coordinates with A, B and C illuminants with the 2° standard observer angle of **1**, **2**, **5**, and **6**.[a]

Compound	State	CIE A			CIE B			CIE C		
		L^*	a^*	b^*	L^*	a^*	b^*	L^*	a^*	b^*
1	neutral	99.0	−2.3	92.3	98.0	−13.9	103.1	97.4	−22.6	106.7
	oxidized	41.5	9.1	−28.9	41.8	14.0	−30.2	42.1	18.2	−30.3
2	neutral	99.3	−1.1	65.8	98.5	−11.1	71.5	98.0	−18.7	73.2
	oxidized	78.5	−2.0	−1.3	78.7	−2.1	−0.9	78.7	−2.0	−0.8
5	neutral	98.8	0.6	4.9	98.7	−0.8	5.6	98.6	−2.0	5.9
	1st oxidation	96.5	6.8	16.5	95.5	6.4	14.7	95.1	5.2	14.0
	2nd oxidation	87.3	−8.5	0.1	87.7	−7.2	0.8	87.8	−6.5	1.1
6	neutral	99.4	−0.6	5.7	99.4	−2.5	6.9	99.3	−3.9	7.4
	1st oxidation	95.5	10.7	15.9	94.3	11.1	13.4	93.8	10.1	12.4
	2nd oxidation	88.1	−1.3	4.1	87.9	0.5	3.4	87.8	1.0	3.1

[a] Calculated for the spectral range 360–830 nm.

Conclusion

It was found that the fluorescence of an intrinsically fluorescent fluorophore consisting of two diphenylamines and a fluorene core was quenched, in part, by its two azomethine bonds. Courtesy of the terminal amines, the fluorophore formed an antiparallel dimer that was connected by two hydrogen bonds. The supramolecular assembly was reinforced by a least three other intermolecular contacts. Intermolecular hydrogen-bonding involving the terminal amine was confirmed experimentally by FTIR, NMR, and X-ray diffraction, and complemented by DFT calculations. Engaging these intermolecular contacts at high concentrations in solution and thin films, along with water-mediated aggregation, resulted in pronounced fluorescence shifts and upwards of an eightfold fluorescence enhancement. Intermolecular contacts can therefore be used to reduce the fluorescence deactivation modes of azomethines and enhance their otherwise quenched fluorescence. The concentration-dependent fluorescence turn-on behavior, coupled with other fluorescence enhancement strategies, would be ideal to completely suppress the intrinsic azomethine fluorescence quenching modes and make the otherwise weakly fluorescent fluorophores extremely fluorescent. Applying these strategies to enhance the thin-film fluorescence of azomethines further would ultimately be beneficial for improving the efficiency of emitting devices.

Experimental Section

Spectroscopy

Absorption spectra were measured with Varian Cary 500 combined UV/Vis/NIR spectrometer. Fluorescence measurements were obtained with an Edinburgh Instruments FLSP-920 combined steady-state time-resolved spectrometer. Solutions for fluorescence and quantum yields measurements were prepared with an absorbance ≤ 0.1 at the corresponding absorption maxima. Prior to measurements, the samples were purged with nitrogen for at least 20 min. Quantum yields were calculated against naphthalene in cyclohexane ($\Phi_{fl} = 0.23$) and correcting for the difference in refractive index of the solvent used for the actinometry and the compound of study.[23]

Theoretical calculations

The ground-state geometry was first optimized by using the X-ray crystallographic coordinates of **1** as the starting point. The geometries were then fully optimized. For the hydrogen-bonding studies, the geometries of both the monomer and hydrogen-bonded dimer were optimized. The calculations were carried out with Gaussian 09. The ground-state geometry optimization of the two systems was performed with DFT with B3LYP as the hybrid functional and 6–31G(d) as the basis set. The electronic transition energies of the monomer and dimer were calculated by using time-dependent DFT with the same functional and basis set.

Electrochemistry

Electrochemical measurements were performed with a multi-channel BioLogic VSP potentiostat. The compounds were dissolved in the corresponding anhydrous and degassed solvent at 10^{-4} M with 0.1 M tetrabutylammonium hexafluorophosphate as the electrolyte. A platinum electrode was used as the working electrode with a platinum wire as the auxiliary electrode. The reference electrode was a silver wire electrode. Ferrocene was added to the solution as an internal reference and the voltammograms were calibrated against its reversible Fc/Fc^+ redox couple.[27]

Spectroelectrochemistry

Spectroelectrochemical measurements were obtained with a potentiostat using a Pt mesh electrode that was placed in a thin-cell spectrometer cell. The mesh, counter, and reference electrodes were all placed in the UV cell that was inserted into a UV/Vis/NIR spectrometer. The electrodes were connected to the potentiostat. Samples were prepared by dissolving the compound of study in the corresponding anhydrous and degassed solvent with 0.1 M tetrabutylammonium hexafluorophosphate as the electrolyte. A platinum mesh working electrode, platinum wire auxiliary electrode, and silver wire reference electrode were used.

Fluoroelectrochemistry

The fluorescence changes at different applied potentials were measured by using a combined steady-state time-resolved spectrometer connected to a potentiostat. The sample was rotated by 45° relative to the excitation beam. The samples were prepared by dissolving the compounds in THF (0.2 mL) and distilled water (1.8 mL) to which was added KCl (15 mg). The solutions were purged with nitrogen for at least 20 min. A platinum mesh working electrode,

platinum wire auxiliary electrode, and silver wire reference electrode were used.

Preparation of thin films and encapsulation

Thin films were prepared by drop-casting dichloromethane solutions of the fluorophores onto glass microscope slides. The thickness of the as-cast film of **2** was 40 nm. Encapsulation of the azomethine in a PMMA matrix ($M_n = 70\,000\ g\,mol^{-1}$) was performed by dissolving the fluorophore and PMMA in 1:10, 1:30, 1:50, 1:80, and 1:100 weight ratios in dichloromethane. The solutions were drop-cast onto glass slides. The thin films deposited had thicknesses of 200 nm (1:10), 150 nm (1:30), 160 nm (1:50), 400 nm (1:80) and 230 nm (1:100).

Synthesis

Compound 3: Diphenylamine (1.30 g, 7.7 mmol), $CsCO_3$ (1.54 g, 8.00 mmol), $Pd(OAc)_2$ (70 mg, 0.31 mmol), and tBu_3P (62 mg, 0.31 mmol) were added to a solution of 2,7-dibromo-9*H*-fluorene (1.00 g, 3.08 mmol) in anhydrous toluene (20 mL). The mixture was heated under a nitrogen atmosphere at 120 °C for 24 h. After cooling, the solvent was evaporated under reduced pressure and the resulting residue was solubilized in CH_2Cl_2 and extracted with water and brine. The organic layer was dried over $MgSO_4$, filtered, and then concentrated. The crude product was purified by column chromatography on silica gel (hexane/CH_2Cl_2, 9:1) to afford the title compound (1.22 g, 79%) as a pale-brown solid. ^{1}H NMR (400 MHz, $CDCl_3$): $\delta = 7.55$ (d, $J = 8.2$ Hz, 2H), 7.26–7.21 (m, 10H), 7.11 (d, $J = 7.8$ Hz, 10H), 6.99 (t, $J = 7.3$ Hz, 4H), 3.72 ppm (s, 2H); ^{13}C NMR (100 MHz, $CDCl_3$): $\delta = 148.2$, 146.4, 144.7, 136.9, 129.3, 124.0, 123.9, 122.6, 121.6, 120.1, 36.9 ppm. HRMS: *m/z* calcd: 500.2247 $[M^*]^+$; found: 500.2258; *m/z* calcd: 501.2325 $[M+H]^+$; found: 501.2337.

Compound 4: Diphenylamine (1.03 g, 6.1 mmol), $CsCO_3$ (1.22 g, 6.32 mmol), $Pd(OAc)_2$ (55 mg, 0.24 mmol), and tBu_3P (50 mg, 0.25 mmol) were added to a solution of 2,7-dibromo-9,9-dihexyl-9*H*-fluorene (1.20 g, 2.44 mmol) in anhydrous toluene (20 mL). The mixture was heated under a nitrogen atmosphere at 120 °C for 24 h. After cooling, the solvent was evaporated under reduced pressure and the residue was solubilized in CH_2Cl_2 and extracted with water and brine. The organic layer was dried over $MgSO_4$, filtered, and then concentrated. The crude product was purified by column chromatography on silica gel (hexane/CH_2Cl_2, 10:1) and the title compound (1.31 g, 80%) was isolated as a white solid. ^{1}H NMR (400 MHz, [D$_6$]acetone): $\delta = 7.64$ (d, $J = 8.2$ Hz, 2H), 7.31–7.25 (m, 8H), 7.15 (d, $J = 1.9$ Hz, 2H), 7.10–7.07 (m, 8H), 7.04–6.98 (m, 6H), 1.89–1.81 (m, 4H), 1.18–1.07 (m, 12H), 0.81 (t, $J = 7.2$ Hz, 6H), 0.75–0.70 ppm (m, 4H); ^{13}C NMR (100 MHz, [D$_6$]acetone): $\delta =$ 152.9, 148.9, 147.6, 137.4, 130.1, 124.6, 124.4, 123.4, 120.9, 120.4, 55.8, 40.8, 32.3, 24.6, 23.2, 14.3 ppm. HRMS: *m/z* calcd: 669.4203 $[M+H]^+$; found 669.4206.

Compound 5: Anhydrous dimethylformamide (2.3 mL) and $POCl_3$ (2.9 mL) were added at 0 °C to a solution of **3** (0.6 g, 1.2 mmol) dissolved in anhydrous 1,2-dichloroethane (5 mL). The mixture was heated to reflux for 15 h under a nitrogen atmosphere and then cooled to RT and neutralized with a saturated solution of $NaHCO_3$. The crude product was extracted with dichloromethane and purified by SiO_2 column chromatography (dichloromethane/hexane, 8:2). The title compound (530 mg, 81%) was isolated as a yellow solid. ^{1}H NMR (400 MHz, $CDCl_3$): $\delta = 9.82$ (s, 2H), 7.72–7.66 (m, 6H), 7.38–7.32 (m, 6H), 7.23–7.15 (m, 8H), 7.03 (d, $J = 8.7$ Hz, 4H), 3.82 ppm (s, 2H); ^{13}C NMR (100 MHz, $CDCl_3$): $\delta = 190.6$, 153.60, 146.4, 145.2, 145.1, 138.5, 131.5, 129.9, 129.3, 126.3, 125.6, 125.2, 123.3, 120.9, 119.6, 37.0 ppm. HRMS: *m/z* calcd: 556.2145 $[M^*]^+$; found: 556.2153; *m/z* calcd 557.2224 $[M+H]^+$; found: 557.2238.

Compound 6: Anhydrous dimethylformamide (1.20 mL) and $POCl_3$ (1.5 mL) were added at 0 °C to a solution of **4** (0.40 g, 0.60 mmol) dissolved in anhydrous 1,2-dichloroethane (10 mL). The mixture was heated to reflux for 15 h under a nitrogen atmosphere and then cooled to RT and neutralized with a saturated solution of $NaHCO_3$. The crude product was extracted with dichloromethane and purified by SiO_2 column chromatography (ethyl acetate/hexane, 1:9). The titled compound (370 mg, 85%) was isolated as a yellow solid. ^{1}H NMR (400 MHz, [D$_6$]acetone): $\delta = 9.84$ (s, 2H), 7.82 (d, $J = 8.1$ Hz, 2H), 7.77–7.72 (d, $J = 8.8$ Hz, 4H), 7.45–7.38 (m, 4H), 7.34 (d, $J = 1.9$ Hz, 2H), 7.25 (dt, $J = 13.9$, 4.3 Hz, 6H), 7.16 (dd, $J =$ 8.1, 2.0 Hz, 2H), 7.05 (d, $J = 8.7$ Hz, 4H), 2.05–1.92 (m, 4H), 1.17–1.07 (m, 12H), 0.81 (t, $J = 7.1$ Hz, 6H), 0.74–0.72 ppm (m, 4H); ^{13}C NMR (100 MHz, [D$_6$]acetone): $\delta = 190.8$, 154.4, 153.8, 147.5, 146.5, 139.1, 132.0, 130.9, 130.6, 127.1, 126.7, 126.2, 122.5, 122.0, 120.1, 56.4, 40.7, 32.4, 29.8, 24.8, 23.3, 14.5 ppm; HRMS: *m/z* calcd: 725.4102 $[M+H]^+$; found: 725.4092.

Compound 1: A catalytic amount of TFA that was diluted in EtOH was added to a solution of **5** (100.7 mg, 0.18 mmol) and **7** (93.4 mg, 0.36 mmol) in anhydrous ethanol (10 mL). The reaction mixture was then heated at 80 °C for 15 h, then the TFA was neutralized by adding a small amount of Et_3N and the solvent was evaporated. The crude product was purified by SiO_2 column chromatography (ethyl acetate/hexane, 4:6 with 1% Et_3N). The title compound (150 mg, 80%) was isolated as a dark-red solid. ^{1}H NMR (400 MHz, $CDCl_3$): $\delta = 7.83$ (s, 2H), 7.57 (d, $J = 8.2$ Hz, 2H), 7.53 (d, $J = 8.8$ Hz, 4H), 7.26–7.20 (m, 6H), 7.11–7.02 (m, 8H), 6.97 (d, $J =$ 8.8 Hz, 4H), 6.24 (s, 4H), 4.33 (q, $J = 7.1$ Hz, 4H), 4.19 (q, $J = 7.1$ Hz, 4H), 3.70 (s, 2H), 1.34 (t, $J = 7.1$ Hz, 6H), 1.25 ppm (t, $J = 7.1$ Hz, 6H); ^{13}C NMR (100 MHz, $CDCl_3$): $\delta = 164.0$, 163.1, 159.5, 150.6, 149.5, 146.1, 144.6, 144.2, 136.8, 132.7, 128.6, 128.4, 128.3, 125.3, 124.4, 123.8, 123.2, 121.5, 120.0, 119.6, 100.5, 59.6, 58.6, 35.6, 12.9, 12.8 ppm; HRMS: *m/z* calcd: 1037.3361 $[M+H]^+$; found: 1037.3337.

Compound 2: A catalytic amount of TFA that was previously diluted in EtOH was added to the solution of **6** (163.4 mg, 0.22 mmol) and **7** (116.4 mg, 0.45 mmol) in anhydrous ethanol (10 mL). The reaction mixture was heated at 80 °C for 15 h, then the TFA was neutralized by adding a small amount of Et_3N and the solvent was evaporated. The crude product was purified by SiO_2 column chromatography (ethyl acetate/hexane, 4:7 with 1% Et_3N) to afford the title compound (165 mg, 61%) as a dark-red solid. ^{1}H NMR (400 MHz, $CDCl_3$): $\delta = 7.90$ (s, 2H), 7.59 (d, $J = 8.8$ Hz, 4H), 7.53 (d, $J = 8.1$ Hz, 2H), 7.33–7.27 (m, 4H), 7.15 (d, $J = 7.6$ Hz, 4H), 7.11–7.02 (m, 10H), 6.26 (s, 4H), 4.38 (q, $J = 7.1$ Hz, 4H), 4.25 (q, $J = 7.1$ Hz, 4H), 1.83–1.73 (m, 4H), 1.40 (t, $J = 7.1$ Hz, 6H), 1.31 (t, $J = 7.1$ Hz, 6H), 1.18–1.01 (m, 12H), 0.81 (t, $J = 7.2$ Hz, 6H), 0.67 ppm (m, 4H); ^{13}C NMR (100 MHz, $CDCl_3$): $\delta = 165.8$, 164.7, 159.2, 152.7, 152.5, 150.6, 147.2, 145.8, 137.2, 135.4, 129.8, 129.6, 129.0, 128.3, 125.2, 124.8, 124.0, 121.5, 120.4, 120.3, 103.2, 61.5, 60.4, 55.3, 40.2, 31.7, 29.6, 23.9, 22.6, 14.5, 14.3, 14.2 ppm; HRMS: *m/z* calcd: 1205.5239 $[M+H]^+$; found: 1205.5237.

Single-crystal structure determination

X-ray diffraction data (Table 4) were collected with a Bruker APEX-II CCD diffractometer with Ga Kα radiation ($\lambda = 1.34139$ Å). The crystal was kept at 100 K during data collection. Using Olex2,[28] the structure was solved with the XT[29] structure solution program using direct methods and refined with the XL[30] refinement package using least-squares minimization. CCDC 1454905 contains the sup-

Table 4. Details of crystal structure determination of **1**.

CCDC	1454905
formula	$C_{59}H_{52}N_6O_8S_2$
M_w [g mol^{-1}]; F(000)	1037.18
crystal color and form	Dark red
crystal size [mm]	0.08×0.08×0.04
T [K]; $d_{calcd.}$ [g cm^{-3}]	100; 1.170
crystal system	monoclinic
space group	$P2_1/c$
unit cell: a [Å]	32.5784(7)
b [Å]	9.0681 (2)
c [Å]	19.9889(4)
α [°]	90
β [°]	94.1330(14)
γ [°]	90
V [Å^3]; Z	5889.8(2); 4
θ range [°]; completeness	4.732 to 121.406; 99.8%
reflections: collected/independent; R_{int}	106070/13529; R_{int} = 0.0969, R_{sigma} = 0.0582
μ [mm^{-1}]	0.824
abs. Corr.	0.937–0.968
$R1$(F); $wR(F^2)$ [I > 2σ(I)]	R_1 = 0.0761; wR_2 = 0.2096
$R1$(F); $wR(F^2)$ (all data)	R_1 = 0.1186; wR_2 = 0.2322
GoF(F^2)	1.039
max. residual e$^-$ density	0.42/−0.30

plementary crystallographic data for this paper. These data can be obtained free of charge from The Cambridge Crystallographic Data Centre.

Acknowledgements

The authors acknowledge both NSERC Canada and the Canada Foundation for Innovation for operating and equipment grants, respectively. M.-H.T. acknowledges the Fonds de recherche du Québec - Nature et technologies for a graduate scholarship. The assistance of Dr. M. Simard is greatly appreciated for the X-ray crystal structure resolution. WestGrid (www.westgrid.ca) and Compute Canada/Calcul Canada (www.computecanada.ca) are both acknowledged for access to software and computational resources. The Center for Self-Assembled Chemical Structures is also acknowledged.

Keywords: conjugation · electrochemistry · fluorescence · solvatochromism · supramolecular chemistry

[1] a) M. L. Petrus, F. S. F. Morgenstern, A. Sadhanala, R. H. Friend, N. C. Greenham, T. J. Dingemans, *Chem. Mater.* **2015**, *27*, 2990 – 2997; b) M. L. Petrus, T. Bein, T. J. Dingemans, P. Docampo, *J. Mater. Chem. A* **2015**, *3*, 12159 – 12162; c) X. Ma, H. Niu, H. Wen, S. Wang, Y. Lian, X. Jiang, C. Wang, X. Bai, W. Wang, *J. Mater. Chem. C* **2015**, *3*, 3482 – 3493.

[2] a) X. Ma, Y. Wu, H. Wen, H. Niu, C. Wang, C. Qin, X. Bai, L. Lei, W. Wang, *RSC Adv.* **2016**, *6*, 4564 – 4575; b) A. Leliège, S. Barik, W. G. Skene, *ACS Appl. Mater. Interfaces* **2014**, *6*, 6920 – 6929; c) L. Sicard, D. Navarathne, T. Skalski, W. G. Skene, *Adv. Funct. Mater.* **2013**, *23*, 3549 – 3559; d) L. Hao, W. Wang, Y. Sun, H. Niu, *J. Electroanal. Chem.* **2015**, *742*, 74 – 83.

[3] a) M. Shyamal, P. Mazumdar, S. Maity, G. P. Sahoo, G. Salgado-Morán, A. Misra, *J. Phys. Chem. A* **2016**, *120*, 210 – 220; b) A. Kathiravan, K. Sundaravel, M. Jaccob, G. Dhinagaran, A. Rameshkumar, D. Arul Ananth, T. Sivasudha, *J. Phys. Chem. B* **2014**, *118*, 13573 – 13581; c) G. Boice, B. O. Patrick, R. McDonald, C. Bohne, R. Hicks, *J. Org. Chem.* **2014**, *79*, 9196 – 9205; d) S. Dufresne, I. U. Roche, T. Skalski, W. G. Skene, *J. Phys. Chem. C* **2010**, *114*, 13106 – 13112; e) N. Kawatsuki, H. Matsushita, T. Washio, J. Kozuki, M. Kondo, T. Sasaki, H. Ono, *Macromolecules* **2013**, *46*, 2092; f) D. Tsang, M. Bourgeaux, W. G. Skene, *J. Photochem. Photobiol. A* **2007**, *192*, 122 – 129.

[4] a) Y. Luo, M. Utecht, J. Dokić, S. Korchak, H.-M. Vieth, R. Haag, P. Saalfrank, *ChemPhysChem* **2011**, *12*, 2311 – 2321; b) Y. Luo, S. Korchak, H.-M. Vieth, R. Haag, *ChemPhysChem* **2011**, *12*, 132 – 135; c) J. Mielke, F. Leyssner, M. Koch, S. Meyer, Y. Luo, S. Selvanathan, R. Haag, P. Tegeder, L. Grill, *ACS Nano* **2011**, *5*, 2090 – 2097; d) L. Greb, J.-M. Lehn, *J. Am. Chem. Soc.* **2014**, *136*, 13114 – 13117; e) P. J. Coelho, M. C. R. Castro, M. M. M. Raposo, *J. Photochem. Photobiol. A* **2013**, *259*, 59 – 65; f) C. Gahl, D. Brete, F. Leyssner, M. Koch, E. R. McNellis, J. Mielke, R. Carley, L. Grill, K. Reuter, P. Tegeder, M. Weinelt, *J. Am. Chem. Soc.* **2013**, *135*, 4273 – 4281.

[5] a) A. Singh, R. Singh, M. Shellaiah, E. C. Prakash, H.-C. Chang, P. Raghunath, M.-C. Lin, H.-C. Lin, *Sens. Actuators B* **2015**, *207*, 338 – 345; b) M. Yang, Y. Zhang, W. Zhu, H. Wang, J. Huang, L. Cheng, H. Zhou, J. Wu, Y. Tian, *J. Mater. Chem. C* **2015**, *3*, 1994 – 2002; c) M. Shellaiah, T. Simon, V. Srinivasadesikan, C.-M. Lin, K. W. Sun, F.-H. Ko, M.-C. Lin, H.-C. Lin, *J. Mater. Chem. C* **2016**, *4*.

[6] a) G. Yang, S. Li, S. Wang, Y. Li, *C. R. Chim.* **2011**, *14*, 789 – 798; b) V. S. Padalkar, S. Seki, *Chem. Soc. Rev.* **2016**, *45*, 169 – 202.

[7] a) J. Mei, N. L. C. Leung, R. T. K. Kwok, J. W. Y. Lam, B. Z. Tang, *Chem. Rev.* **2015**, *115*, 11718 – 11940; b) W. Lingyun, Y. Lingling, C. Derong, *Curr. Org. Chem.* **2014**, *18*, 1028 – 1049; c) L. Zhu, Y. Zhao, *J. Mater. Chem. C* **2013**, *1*, 1059 – 1065; d) S. S. Babu, K. K. Kartha, A. Ajayaghosh, *J. Phys. Chem. Lett.* **2010**, *1*, 3413 – 3424; e) L. Wang, G. Fang, D. Cao, *J. Macromol. Sci. Pure Appl. Chem.* **2014**, *51*, 668 – 681; f) J. Chen, B. Z. Tang, *Restricted Intramolecular Rotations: A Mechanism for Aggregation-Induced Emission, in Aggregation-Induced Emission: Fundamentals and Applications, Volumes 1 and 2* (Eds.: A. Qin, B. Z. Tang), John Wiley and Sons Ltd, **2013**, pp. 307 – 322; g) Y. Q. Dong, C. Li, W. Zhao, Y. Dong, B. Z. Tang, *J. Molecul. Eng. Mater.* **2013**, *1*, 1340010/1 – 1340010/13.

[8] M. Tsuchimoto, N. Yoshida, A. Sugimoto, N. Teramoto, K. Nakajima, *J. Mol. Struct.* **2016**, *1105*, 152 – 158.

[9] a) Z. Chen, J. Liang, X. Han, J. Yin, G.-A. Yu, S. H. Liu, *Dyes Pigm.* **2015**, *112*, 59 – 66; b) S. J. Ananthakrishnan, E. Varathan, N. Somanathan, V. Subramanian, A. B. Mandal, J. D. Sudha, R. Ramakrishnan, *J. Mater. Chem. C* **2014**, *2*, 9035 – 9044.

[10] a) C.-W. Lin, C.-T. Chen, *AIE or AIEE Materials for Electroluminescence Applications, in Aggregation-Induced Emission: Fundamentals and Applications*, Volumes 1 and 2, John Wiley and Sons Ltd, **2013**, pp. 1 – 41; b) Y. Gong, Y. Zhang, W. Z. Yuan, J. Z. Sun, Y. Zhang, *J. Phys. Chem. C* **2014**, *118*, 10998 – 11005; c) S. Jin, Y. Tian, F. Liu, J. Chen, S. Deng, N. Xu, *J. Mater. Chem. C* **2015**, *3*, 8066 – 8073; d) S. Kamino, A. Muranaka, M. Murakami, A. Tatsumi, N. Nagaoka, Y. Shirasaki, K. Watanabe, K. Yoshida, J. Horigome, S. Komeda, M. Uchiyama, S. Enomoto, *Phys. Chem. Chem. Phys.* **2013**, *15*, 2131 – 2140; e) C. Coya, C. Ruiz, A. L. Alvarez, S. Alvarez-Garcia, E. M. Garcia-Frutos, B. Gomez-Lor, A. de Andres, *Org. Electron.* **2012**, *13*, 2138 – 2148; f) S. J. Ananthakrishnan, E. Varathan, V. Subramanian, N. Somanathan, A. B. Mandal, *J. Phys. Chem. C* **2014**, *118*, 28084 – 28094.

[11] B.-K. An, J. Gierschner, S. Y. Park, *Acc. Chem. Res.* **2011**, *44*, 544 – 554.

[12] J. W. Chung, S.-J. Yoon, B.-K. An, S. Y. Park, *J. Phys. Chem.* **2013**, *117*, 11285 – 11291.

[13] a) W. Luo, Y. Zhu, J. Zhang, J. He, Z. Chi, P. W. Miller, L. Chen, C.-Y. Su, *Chem. Commun.* **2014**, *50*, 11942 – 11945; b) Y. Cao, M. Yang, Y. Wang, H. Zhou, J. Zheng, X. Zhang, J. Wu, Y. Tian, Z. Wu, *J. Mater. Chem. C* **2014**, *2*, 3686 – 3694.

[14] S. Chopra, N. Singh, P. Thangarasu, V. K. Bhardwaj, N. Kaur, *Dyes Pigm.* **2014**, *106*, 45 – 50.

[15] C. Mallet, C. Moussallem, A. Faurie, M. Allain, F. Gohier, W. G. Skene, P. Frère, *Chem. Eur. J.* **2015**, *21*, 7944 – 7953.

[16] S. Pramanik, V. Bhalla, M. Kumar, *ACS Appl. Mater. Interfaces* **2015**, *7*, 22786 – 22795.

[17] L. Wang, Z. Zheng, Z. Yu, J. Zheng, M. Fang, J. Wu, Y. Tian, H. Zhou, *J. Mater. Chem. C* **2013**, *1*, 6952 – 6959.

[18] a) A. Priimagi, J. Vapaavuori, F. J. Rodriguez, C. F. J. Faul, M. T. Heino, O. Ikkala, M. Kauranen, M. Kaivola, *Chem. Mater.* **2008**, *20*, 6358 – 6363; b) D. González-Rodríguez, A. P. H. J. Schenning, *Chem. Mater.* **2011**, *23*, 310 – 325; c) S. Yagai, K. Iwai, M. Yamauchi, T. Karatsu, A. Kitamura, S. Uemura, M. Morimoto, H. Wang, F. Würthner, *Angew. Chem. Int. Ed.*

2014, *53*, 2602 – 2606; *Angew. Chem.* **2014**, *126*, 2640 – 2644; d) S. Yagai, T. Karatsu, A. Kitamura, *Chem. Eur. J.* **2005**, *11*, 4054 – 4063; e) N. H. Damrauer, J. M. Hodgkiss, J. Rosenthal, D. G. Nocera, *J. Phys. Chem. B* **2004**, *108*, 6315 – 6321; f) A. P. H. J. Schenning, J. v. Herrikhuyzen, P. Jonkheijm, Z. Chen, F. Würthner, E. W. Meijer, *J. Am. Chem. Soc.* **2002**, *124*, 10252 – 10253; g) H. Kar, S. Ghosh, *Chem. Commun.* **2014**, *50*, 1064 – 1066; h) M. Shellaiah, Y. C. Rajan, H.-C. Lin, *J. Mater. Chem.* **2012**, *22*, 8976 – 8987; i) M. Shellaiah, M. V. Ramakrishnam Raju, A. Singh, H.-C. Lin, K.-H. Wei, H.-C. Lin, *J. Mater. Chem. A* **2014**, *2*, 17463 – 17476; j) C. B. Aakeröy, A. M. Beatty, B. A. Helfrich, *Angew. Chem. Int. Ed.* **2001**, *40*, 3240 – 3242; *Angew. Chem.* **2001**, *113*, 3340 – 3342.

[19] A. Bolduc, C. Mallet, W. G. Skene, *Sci. China Chem.* **2013**, *56*, 3 – 23.

[20] J. Gierschner, L. Lüer, B. Milián-Medina, D. Oelkrug, H.-J. Egelhaaf, *J. Phys. Chem. Lett.* **2013**, *4*, 2686 – 2697.

[21] F. Würthner, T. E. Kaiser, C. R. Saha-Möller, *Angew. Chem. Int. Ed.* **2011**, *50*, 3376 – 3410; *Angew. Chem.* **2011**, *123*, 3436 – 3473.

[22] a) I. M. Smallwood, *Handbook of Organic Solvent Properties*, **1996**; b) J. A. Riddick, W. B. Bunger, T. K. Sakano, *Organic Solvents: Physical Properties and Methods of Purification*, Wiley, New York, **1986**.

[23] A. M. Brouwer, *Pure Appl. Chem.* **2011**, *83*, 2213 – 2228.

[24] J. R. Lakowicz, *Principles of Fluorescence Spectroscopy*, 3rd ed., Springer, New York, **2006**.

[25] G.-J. Zhao, K.-L. Han, *ChemPhysChem* **2008**, *9*, 1842 – 1846.

[26] *CIE Technical Report on Colorimetry, Commission Internationale de L'Éclairage 2004* CIE 15:2004 79, 72 pages.

[27] N. G. Connelly, W. E. Geiger, *Chem. Rev.* **1996**, *96*, 877 – 910.

[28] O. V. Dolomanov, L. J. Bourhis, R. J. Gildea, J. A. K. Howard, H. Puschmann, *J. Appl. Crystallogr.* **2009**, *42*, 339 – 341.

[29] G. Sheldrick, *Acta Crystallogr. Sect. A* **2015**, *71*, 3 – 8.

[30] G. Sheldrick, *Acta Crystallogr. Sect. A* **2008**, *64*, 112 – 122.

Received: February 23, 2016
Revised: April 11, 2016
Published online on ■■ ■■, 0000

FULL PAPER

Turn on the lights! The fluorescence of an electrochromic azomethine, quenched by its conjugated imines, can be enhanced by activating supramolecular intra- and intermolecular contacts (see figure). The enhanced fluorescence can also be switched off and on electrochemically.

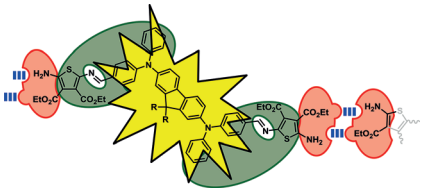

Fluorescence Enhancement

*M. Wałęsa-Chorab, M.-H. Tremblay, W. G. Skene**

■■ – ■■

Hydrogen-Bond and Supramolecular-Contact Mediated Fluorescence Enhancement of Electrochromic Azomethines